LETTER

Defect Tolerance in Methylammonium Lead Triiodide Perovskite

K. Xerxes Steirer,* Philip Schulz, Glenn Teeter, Vladan Stevanovic, Mengjin Yang, Kai Zhu, and Joseph J. Berry*

National Renewable Energy Laboratory, Golden, Colorado 80401, United States

S *Supporting Information*

ABSTRACT: Photovoltaic applications of perovskite semiconductor material systems have generated considerable interest in part because of predictions that primary defect energy levels reside outside the bandgap. We present experimental evidence that this enabling material property is present in the halide-lead perovskite, $CH_3NH_3PbI_3$ (MAPbI$_3$), consistent with theoretical predictions. By performing X-ray photoemission spectroscopy, we induce and track dynamic chemical and electronic transformations in the perovskite. These data show compositional changes that begin immediately with exposure to X-ray irradiation, whereas the predominant electronic structure of the thin film on compact TiO_2 appears tolerant to the formation of compensating defect pairs of V_I and V_{MA} and for a large range of I/Pb ratios. Changing film composition is correlated with a shift of the valence-band maximum only as the halide−lead ratio drops below 2.5. This delay is attributed to the invariance of MAPbI$_3$ electronic structure to distributed defects that can significantly transform the electronic density of states only when in high concentrations.
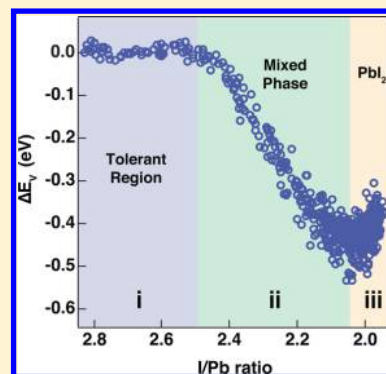
A rapid rise in the use of metal-halide perovskites for photovoltaic (PV) devices with reported efficiencies exceeding 20% promises to enable massive reductions in cost via the use of solution processing approaches.[1] Experimental studies of $CH_3NH_3PbI_3$ (MAPbI$_3$) have demonstrated a range of interesting physical properties that enable high performance in PV and optoelectronic applications. However, an accurate understanding of defect formation processes is required to control the material stability.[2] Approaches to enhance stability of device performance may be linked to the design of specific charge-carrier extraction and encapsulation layers,[3−5] but it remains unclear to what extent intrinsic defects in the absorber layer deteriorate the device performance and lead to instability.

Zhang, Wei, and Zunger initially posed the concept of defect pair tolerance in semiconductors to explain the high tolerance (~1%) of CuInSe$_2$ to native defects.[6] Conceptually, the electronic energy levels of native point defects in such a material system, including vacancies, reside outside the electronic gap. This idea has been theoretically examined by Yang et al. to show that donor−acceptor charge compensation self-regulates for pinned defect formation energies.[7] It has been hypothesized that PV-relevant hybrid perovskite systems are such ionic semiconductors, which exhibit this and other types of defect-tolerant properties. This makes them of interest not only to PV but also particularly compelling for a range of optoelectronic applications when considering their split band structure[8] and low exciton binding energies.[9] While these predictions have motivated synthesis of new materials,[10,11]

defect tolerance has thus far only been theorized for hybrid perovskites materials based on studies using ab initio density functional theory (DFT) and thermodynamic simulations of ionic defects.[12−14] The ionic nature of MAPbI$_3$ is predicted to decouple partially disordered Schottky-type defects from the electronic structure by self-compensation and their energy-level positions in the bands. Theoretical treatments attribute advantageous defect structures to the high ionicity of MAPbI$_3$ and strong Pb lone-pair s orbital and iodine p orbital antibonding coupling. As a result, structural defects including iodine and methylammonium (MA) vacancies have energy levels that fall within the MAPbI$_3$ conduction and valence bands, respectively.[13] Within the cubic MAPbI$_3$ structure ($pm\overline{3}m$), the self-regulation of V_{MA} and V_I results in overall charge neutrality. In more covalent semiconductors such as CdTe and Cu$_2$ZnSnS$_4$, native point defects result in active electronic defect structures with energy levels in the gap.[15,16] The result of reported predictions is that the charge imbalance formed from the loss of a MA cation could be compensated by the loss of an iodine anion. As defects are added, this effect can preserve the electronic structure at the band edges, in the vicinity of the Fermi level, and thus the perovskite semiconducting properties. The concept of defect tolerance should not be confused for defect immunity within the material, as the generation of defects within the conduction and valence bands

is not without consequence (e.g., changes in above gap absorption). Rather, in a defect tolerant system the impact of a significant density of defects is mitigated thus preserving the functional material property. In the case of MAPbI$_3$, it appears the electronic properties of the material are substantially tolerant to the formation of defects within the system, providing process and performance robustness consistent with PV literature on these materials.

Several reports have examined the modulation or degradation of the optoelectronic properties of MAPbI$_3$ and related perovskite systems. Indeed, MAPbI$_3$ has been described as an intrinsically unstable material by Wei and co-workers.[17] Matsumoto et al. examined the photoinduced degradation of MAPbI$_3$ in ambient conditions and found that optical signatures indicating transformation to PbI$_2$ correlated with catastrophic device failure.[18] Similarly, phase decomposition based on loss of the organic cation has been tracked in a number of studies using X-ray diffraction, ultraviolet−visible (UV−vis) spectroscopy, and similar techniques. Ndione et al. have studied substrate effects on ambient MAPbI$_3$ degradation, although effects of the X-rays themselves were not addressed.[19] Xiao et al. have examined the impact of high-energy electron-beam irradiation on defect formation in perovskites.[20] Although these and other published studies have examined changes to the optical and structural properties of MAPbI$_3$ materials, along with correlations to device performance,[4] the quantitative dependence of critical MAPbI$_3$ material properties on defect densities has not been established definitively.

X-ray photoemission spectroscopy (XPS) is extremely useful for the examination of electronic and chemical material properties. However, to date, no study has emerged showing the X-ray-induced effects on organometallic hybrid perovskite materials. Under ultrahigh-vacuum (UHV) conditions at elevated sample temperatures, XPS has previously shown an increase in the rate of metallic lead and PbI$_2$ formation. This evolution was ascribed to PbI$_2$ nucleation and growth.[21] A report by Philippe et al. showed the decomposition of MAPbI$_3$ already occurring at low temperature (∼100 °C), with suggestions that ambient humidity is a contributing factor in this process.[22] Also, it has been observed that X-ray exposure can lead to a shift of the Fermi level in MAPbI$_3$ films on top of nickel oxide substrates.[23] The origin of these altered materials properties remained unclear but could stem from X-ray induced compositional degradations. Remarkably, a later study by Emara et al. showed a dependence of ionization energy on film stoichiometry.[24] Examination by Alberti et al. indicated the formation of metallic lead in MAPbI$_3$ films during exposure to vacuum conditions.[21] In a separate report the formation of metallic lead clusters was ascribed to a radiolysis process and tracked by electron spin resonance spectroscopy.[25] In our examination we have also observed the emergence of metallic lead but find that its presence can be a strong function of the procedure used for material preparation and was mitigated by the material preparation used in this study (see Experimental Methods for details). In particular, compositional stability was observed under UHV conditions over several days.

Here, we report direct observation of the insensitivity of the MAPbI$_3$ electronic structure as a function of compositional changes induced by exposure to monochromatic 1486.6 eV X-ray irradiation during XPS measurements. Probing with X-rays provides systematic alteration and in situ examination of the transformation of MAPbI$_3$ to PbI$_2$. Dynamic XPS data provides experimental evidence for the robustness of the electronic

structure of MAPbI$_3$ under compositional change. More specifically, we propose that methylammonium and iodine vacancy defect pairs are generated, and we investigate their influence on the valence band density of states (DOS) and Fermi level position. Based on analysis of the atomic I/Pb ratio, the critical density of defect tolerance is determined to be one-sixth of the sublattice sites. Beyond this threshold, significant electronic and compositional changes occur within the material.

XPS measurements were conducted on MAPbI$_3$ films on top of compact TiO$_2$ covered FTO substrates. In the experiment, degradation processes associated with X-ray irradiation (1.5 × 10^{11} photons cm^{-2} s^{-1}) induce chemical transformations in the thin film, while photoelectron energy analysis simultaneously monitors the resulting composition, chemical states, and electronic changes in the near-surface region (∼7 nm at 1 keV electron kinetic energy). Experiments were undertaken in UHV with operating pressure at 2 × 10^{-10} Torr, which eliminates ambient atmospheric effects associated with water and oxygen. Each set of XPS spectra was collected over the timespan of 300 s and was continuously repeated over the course of 2 days. Composition calculations have ∼10% absolute uncertainty for each element. However, relative errors for repeated measurements are close to 1% for each region because sample environment, position, and measurement conditions remained unchanged. No oxygen was detected in the samples. XRD measurements on identical samples showed no initial diffraction peak indicative of PbI$_2$ in the as prepared films (Figure S1).

Loss of nitrogen from the film appears to be a primary effect of the X-rays on MAPbI$_3$. Decomposition of the XPS N 1s spectra is depicted in Figure 1. Figure 1a shows that initially, spectral contributions are due only to the MA cation bound in the MAPbI$_3$ structure (MA, 402.6 eV). Upon increasing X-ray exposure, the emission and partial conversion of the MA (CH$_3$NH$_3$$^+$) into methylamine (CH$_3NH_2$) as indicated by the emergence of N$_i$ centered at 401.0 eV then followed by N$_{ii}$ at 399.7 eV. Perovskite degradation into these molecular species has been discussed in detail by Calloni et al.[26] A similar result can be deduced from the C 1s spectra (Figure S2), which exhibit two strong line shapes associated with MA and CH$_3$I but may be obscured by adventitious C compounds. This has been discussed by Liu et al.[27] The fitted N 1s peak area intensity from perovskite MA is shown to fall exponentially over time in Figure 1b. Although MA byproduct formation is clearly observed, the majority of cation species are emitted from the structure resulting in the loss of MA and subsequent vacancy (V$_{MA}$) formation. This is corroborated by the MA-related C 1s spectral intensity also dropping over time. The MA component of the N 1s peak is fit well by a single exponential decay with a time constant of 9.8 h, indicating that the decay process obeys first-order kinetics.

The fitted N 1s spectra and MA decay provide further insight into the thin-film transformation from Avrami phase-change analysis (Figure S3),[28] which has been successfully applied to inorganic thin-film perovskites.[29] The Avrami exponent provides the reaction order and varies with the time dependence of nucleation, growth, and geometry of a material's phase transformation. The reaction order, n, is found to be close to unity and indicates that within the sampling volume a constant nucleation of V$_{MA}$ (depletion of MA) is likely. Avrami described this behavior as a surrounding fluid phase with grains that "rebuff each other".[28] For MAPbI$_3$, this effect may be due to mobile MA$^+$ and I$^-$ ions in the lattice. Higher orders (up to
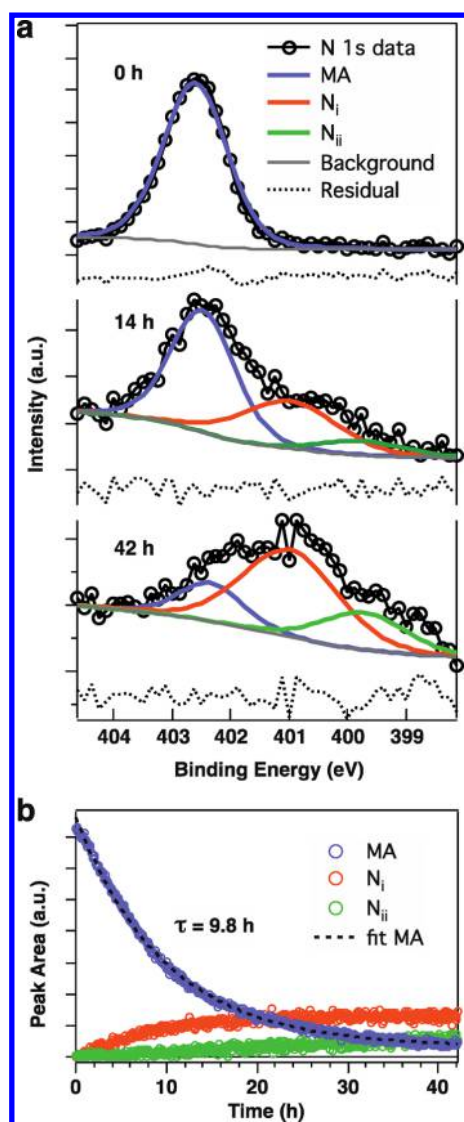
Figure 1. XPS data showing loss of MA cations from MAPbI$_3$. (a) Spectral decomposition of N 1s spectra for initial and extended X-ray exposure. Intensities shown are normalized. (b) Evolution of MA and degradation product signals during continuous X-ray exposure. First-order kinetics resulting in the loss of MA is supported by a single exponential fit with time constant indicated.

four) would indicate expanding nitrogen-depleted regions, which is not observed. The atomic N concentration was invariant to the electron takeoff angle, indicating V_{MA} uniformity perpendicular to the thin film (Figure S4). Hence, the X-ray-induced depletion of MA from MAPbI$_3$ is homogeneous within the measured volume.

Spectral intensities of Pb 4f$_{7/2}$ and I 3d$_{5/2}$ core levels in Figure 2a indicate a transformation of the perovskite thin film to PbI$_2$. Initially, the observed I/Pb ratio is 2.8. This value is low considering the stoichiometric value of 3.0 for MAPbI$_3$. However, repeated XPS studies of films made following the one-step method initiate with I/Pb values between 2.7 and 3.1. These observed values are hypothesized to be affected by slight variations in the ambient conditions in which the samples were prepared. Like that of the MA, although slightly lower, the I/Pb ratio follows a first-order decay kinetic time constant of 8.4 h. The loss of I from MAPbI$_3$ closely follows the loss of MA and suggests a coupled loss mechanism resulting in the simulta-

neous formation of V_{MA} and V_I. Note that the Pb 4f$_{7/2}$ spectra for increasing X-ray exposure (Figure S5) indicate the formation of a small amount of reduced lead (Pb^0) that saturates at a value of 1.7% of the total lead intensity. A much larger spectral response of Pb^0 reported by Alberti et al.[21] was not observed for the MAPbI$_3$ using the one-step method for material preparation. Visual inspection of the sample area exposed to X-ray irradiation for 42 h showed a yellow film and confirms the stimulated transformation of MAPbI$_3$ into PbI$_2$ over the whole film thickness. UV−vis transmission measurements on X-ray degraded areas (Figure S6) indicate the erosion of the MAPbI$_3$ optical gap. The absorption for wavelengths above an onset of 475 nm persists as the PbI$_2$ content in the film increases. These results show that the observed degradation is not purely a surface effect and exhibit similarities to reports of bulk decomposition of organic lead halide perovskite materials under moisture-containing ambient conditions.[18]

Based on the Avrami temporal exponent of unity and the similar loss of I and MA, simultaneous and homogeneously distributed V_{MA} and V_I formation is likely. Indeed, Figure 2b provides evidence that the paired vacancy defects do not disrupt the chemical environment of the MAPbI$_3$ for the first 4.5 h of X-ray exposure (region i in Figure 2b). Above the I/Pb ratio of 2.5, the full-width at half-maximum (fwhm) values for Pb 4f$_{7/2}$ and I 3d$_{5/2}$ are invariant at 0.94 and 1.21 eV, respectively. However, after 4.5 h of X-ray exposure, a sharp increase in the fwhm is observed (region ii in Figure 2b) and correlates with decomposition of the Pb 4f$_{7/2}$ and I 3d$_{5/2}$ spectra, indicating the emergence of a new chemical state associated with PbI$_2$ (see also Figures S7 and S8). Confirmation of this second phase is indicated by the near-perfect isosbestic points in Figure 2c,d. These isosbestic points deviate slightly because of the open-system conditions and loss of material.

Initial disruption of the MAPbI$_3$ structure leads to the observed increase of fwhm. Hence, the I/Pb ratio dictates at what composition the defects begin to interact. For prolonged X-ray exposure, the MAPbI$_3$ almost completely degenerates into PbI$_2$ and the fwhm returns to a low intrinsic line width (region iii in Figure 2b).

The observed chemical transformation of MAPbI$_3$ to PbI$_2$ produces a remarkable trend in the perovskite's electronic structure. Core level peaks are shown versus X-ray exposure time in Figure 3a. These values are superimposed with the valence band maximum relative to its initial energy level (ΔE_v). With respect to the Fermi level (E_F), accurate determination of the valence level ($E_v - E_F$) depends on the fitting procedure and underscores an active area of perovskite research. For example, linear extrapolation results in the initial valence position of 1.6 eV, while on the other hand, a semilogarithmic fit results in $E_v - E_F$ of 1.2 eV.[5,31] Using either fitting protocol, the measured ΔE_v is unaffected. The valence spectral region is also mapped in Figure 3b with temporal axes aligned. Although the stoichiometry of the MAPbI$_3$ varies in region i (Figure 2a,b) following the loss of MA and I, the I 3d$_{5/2}$ and Pb 4f$_{7/2}$ core levels remain stable at 619.52 and 138.69 eV during this time period. These observed centroid positions are in agreement with previous MAPbI$_3$ XPS studies, as shown in Table 1.[21,22,26,30] Note that Alberti et al. reported a dominant molar fraction of PbI$_2$ in their films. Regarding the present case, despite a large change in the I/Pb ratio from 2.8 down to 2.5, the chemical bonding and Fermi level appear unaffected because of the strong electronic coupling between the lead and
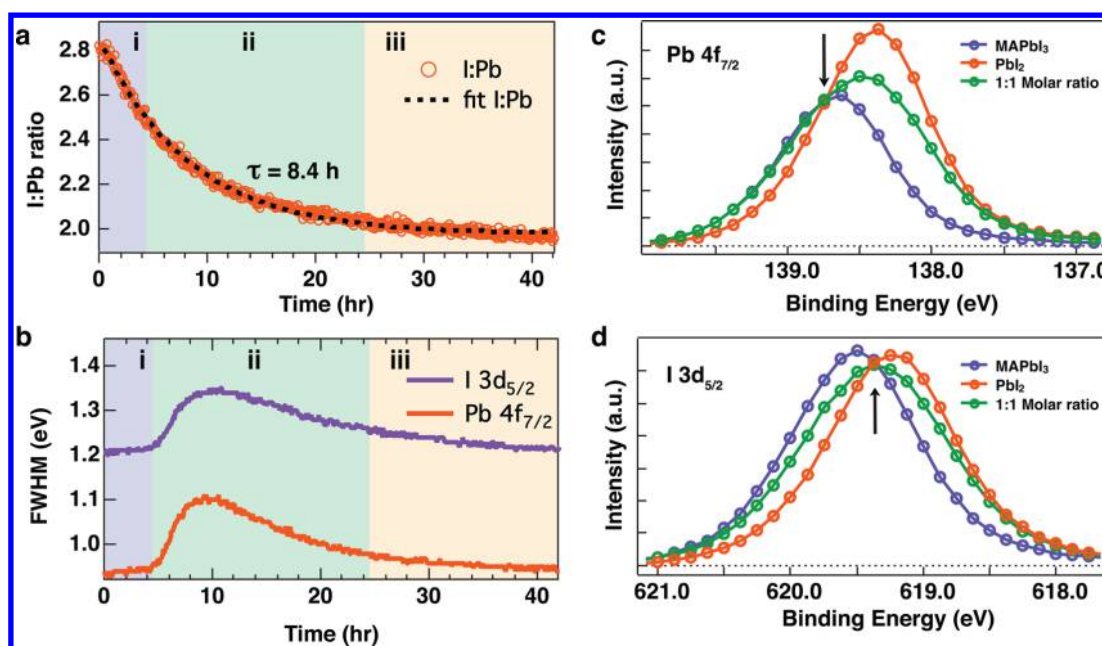
Figure 2. Delayed decomposition during transformation of MAPbI$_3$ to PbI$_2$. (a) Calculated I/Pb ratios from I 3d$_{5/2}$ and Pb 4f$_{7/2}$ core-level spectra. Region i represents defect tolerant MAPbI$_3$; region ii is a mixture of MAPbI$_3$ and PbI$_2$ phases; and region iii is over 90% PbI$_2$. (b) Core levels I 3d$_{5/2}$ and Pb 4f$_{7/2}$ shown in full-width at half-maximum (fwhm) across regions i–iii related to I/Pb ratio during extended monochromatic Al Kα X-ray exposure. (c) Measured Pb 4f$_{7/2}$ core levels shown for 0 h (MAPbI$_3$), 42 h (PbI$_2$), and at 9.0 h (1:1 molar ratio) where spectral decomposition is used in ratio determination. Isosbestic point is indicated by black arrow. (d) Data for 0 h (MAPbI$_3$), 42 h (PbI$_2$), and at 9.0 h (1:1 molar ratio) for I 3d$_{5/2}$ peaks with isosbestic point indicated by black arrow.

iodine atoms in the ionic perovskite. According to the spectral decomposition (Figures S7 and S8), a 1:1 molar ratio of MAPbI$_3$ and PbI$_2$ is formed after 9.04 h of X-ray exposure. By this rationale, a 1:1 linear combination of the initial and final valence-band spectra should fit the valence spectra taken at this point in the experiment. Figure 3c shows the efficacy of this approach, and in principle the entire valence band data set can now be predicted. Hence, after 42 h of X-ray exposure, $E_v - E_F$ shifts by −0.4 eV.

Looking again at Figure 3a, the effect on the valence band is replicated in the XPS core levels reaching a maximum shift near 24 h when the I/Pb ratio has decreased to 2.05. At this point, over 90% of the material is PbI$_2$. In this region, the observed E_v shift to lower binding energy is a superposition of two effects, an increasing bandgap and a shifting Fermi level. The bandgap increases from 1.6 eV for MAPbI$_3$ to 2.3 eV for PbI$_2$, which would result in a shift of E_v to higher binding energy if the Fermi level were at mid gap for the MAPbI$_3$. Here, the MAPbI$_3$ surface Fermi level is close to the conduction band minimum (E_C) likely because of the TiO$_2$ substrate following similar reports.[31,23]

As the defects are generated, the density of states is initially not altered at the band edge for I/Pb values between 2.8 and 2.5. Once changes begin to impact the DOS, the XPS data indicates that the changes are the result of the presence of two distinct components. Because the relative values for $E_v - E_F$ differ for PbI$_2$ and MAPbI$_3$, as soon as PbI$_2$ begins to coexist with MAPbI$_3$, there are two different material contributions to the valence spectra, corresponding to two distinct DOS within the XPS detection volume. This effect dominates the spectral evolution from n-type MAPbI$_3$ to intrinsic PbI$_2$. This point is made clearly when plotting the valence band shift versus I/Pb and is shown in Figure 4. Region i shows a valence band with a wide I/Pb tolerance. In region ii, below I/Pb values of 2.5, the

PbI$_2$ phase emerges and contributes to the apparent shift in valence-band onset. In region iii, the valence-band spectrum is dominated by PbI$_2$.

Above, the data support the conclusion that the MAPbI$_3$ valence band structure is unperturbed by the simultaneous loss of equivalent mole fractions of MA cations and I anions over a remarkably broad range of compositions. Moreover, the three primary regions in Figures 2–4 are represented in optical differences as the initially tolerant MAPbI$_3$ in region i begins to form some PbI$_2$ in region ii and then transforms to PbI$_2$ in region iii. Hence, the bulk of the film is well represented by the XPS data. However, we stress that while XPS measurements in region i show stable valence, Fermi, and core levels, changes to the conduction band are not measured and could be strongly affected. The pairing of V$_{MA}$ and V$_I$ explains the observed electronic resilience to variations in perovskite composition and degradation that follows extended X-ray exposure. Pairing of these defects maintains charge neutrality as theoretically predicted by Wei and co-workers.[7] These predictions indicate the ionicity of the semiconductor, coupled with its chemical makeup, places these defects outside of the semiconductor gap and energetically confines them to their respective bands. Based on our experimental data, these defects seem to form apart from each other in a uniform manner such that their high density does not produce a significant change to the density of states above the I/Pb threshold of 2.5. On the other hand, I/Pb values below 2.5 appear to force V$_{MA}$ and V$_I$ defect pairs to interact in the lattice. Hence, below the 2.5 I/Pb limit, the defect pairs are no longer a subpopulation and will interact to form a secondary phase, PbI$_2$. This is commensurate with the PbI$_2$ contributions to the observed core-level and valence-band spectra. These results acquired in UHV conditions help to explain degradation of solar cells in operational conditions reported by Matsumoto et al. In their study, the MAPbI$_3$-based
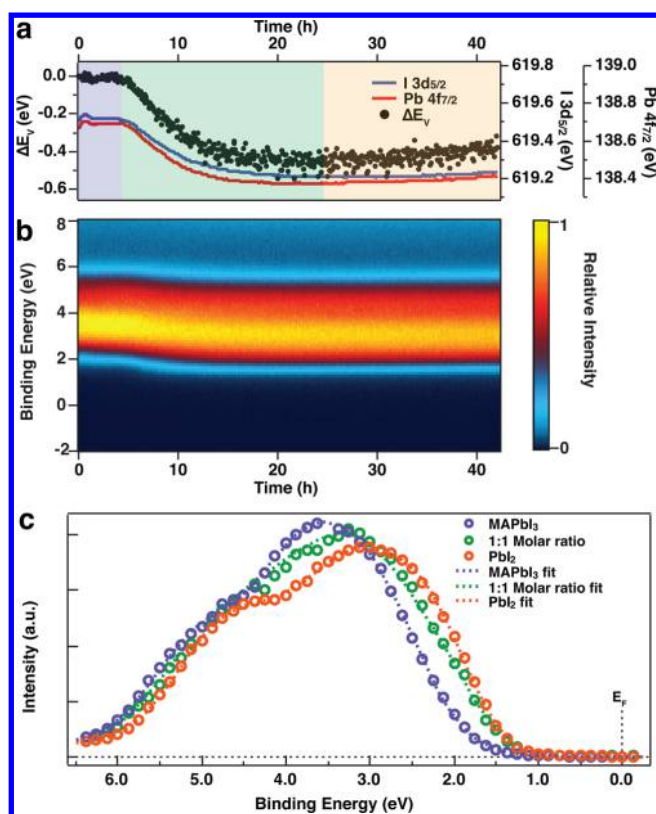
Figure 3. Evolution of electronic structure during transition from MAPbI$_3$ to PbI$_2$. (a) Pb 4f$_{7/2}$ and I 3d$_{5/2}$ core-level spectral peak positions and change in valence band maximum (ΔE_v) over the entire data range. (b) Surface plot of intensity versus time for XPS valence-region spectra. (c) Valence-region spectra at 0 h (MAPbI$_3$) and 42 h (PbI$_2$) used as basis to predict 1:1 molar ratio valence spectra (at 9.0 h). Good overlap is achieved. Note in panel a that E_v and core-level maxima follow similar binding energy shifts.

Table 1. Comparison of Current XPS Results with Earlier Reports

region	MAPbI$_3$ core and valence levels (eV)				
	current work	Alberti et al.[21]	Philippe et al.[22]	Calloni et al.[26]	Schulz et al.
I 3d$_{5/2}$	619.5	618.7	619.4	619.7	619.4[a]
Pb 4f$_{7/2}$	138.7	137.8	138.6	138.9	138.5
E_v−E_F	1.6	n/a	1.55	1.7	1.45

[a]Personal communication.

devices were tolerant to compositional changes leading up to a point (region i, Figure 4) where rapid catastrophic device failure was observed in accordance with an emergence of PbI$_2$ (region ii, Figure 4).[18] The smaller fractions of MA byproducts that emerge during X-ray exposure appear not to strongly affect the valence band edge or Fermi level. The presence and homogeneity of the byproducts support predictions of their occurrence and high mobility made by Yin et al.[13] and Yuan et al.,[32] respectively.

Ionic compensation of point defects in MAPbI$_3$ has been theorized to self-regulate charge carrier concentrations based on thermodynamic calculations by Walsh et al.[12] The experimental data shown here support this defect-tolerance hypothesis with evidence that the predominant electronic structure is not measurably altered by the presence of extraordinarily high defects concentrations. The observation
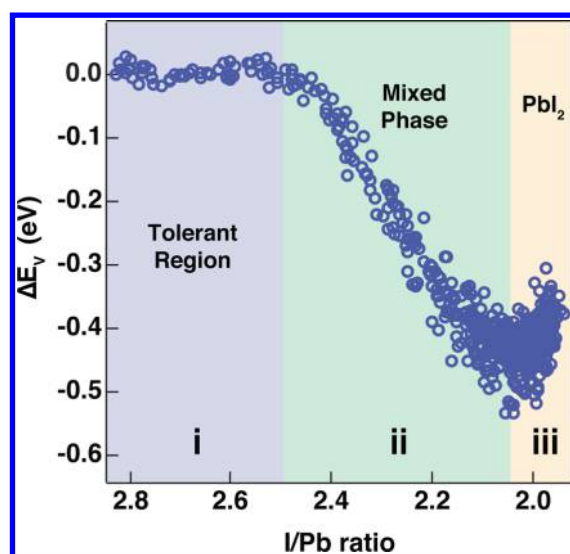
Figure 4. Electronic defect tolerance in MAPbI$_3$. Valence band shift relative to the Fermi level is plotted against the I/Pb ratio. Tolerance to self-regulating defect pairs ($V_{MA} + V_I$) results in a large allowable I/Pb region (i). As defect densities overcome the tolerance level, a mixed phase emerges (ii) and progresses toward PbI$_2$ formation (iii).

of MAPbI$_3$ having tolerance at essentially one defect pair per octahedron is likely unique to ionic semiconductors in contrast to more covalent semiconductors that are typically quite sensitive to defects. Indeed, MAPbI$_3$ may be similar to some defect-tolerant solid oxide fuel cell (SOFCs) materials, which maintain defect tolerance to anion vacancies without performance loss, until concentrations increase to the point that defect electronic states delocalize and interact.[33] Furthermore, Avrami analysis (Figure S3) indicates that in the defect-tolerant regime, point defects are uniformly dispersed and suggests the possible formation of an ordered vacancy compound, although additional experiments are required to verify this hypothesis.

In conclusion, the effects of paired defects on MAPbI$_3$ via in situ XPS over tens of hours have been elucidated. These results are consistent with theoretical predictions and indicate that these materials are extremely tolerant to self-compensating V_{MA} and V_I point defect pairs. Additionally, these results are important for those performing XPS or similar photoemission-based characterization on halide perovskites. The generation of defects and subsequent degradation of these materials under XPS measurement conditions is critical to account for because we have observed similar effects in related perovskite compounds such as HC(NH$_2$)$_2$PbI$_3$. Perovskite defect tolerance with respect to stoichiometric loss of MA + I species appears to result from the V_{MA} and V_I donor- and acceptor-type defects falling very close to or within their respective bands. This direct observation of the unique defect properties of this material will help guide measurement and development of the next generation of perovskite semiconductor alloys.

■ EXPERIMENTAL METHODS

Film Formation. A compact TiO$_2$ layer was deposited onto a base-bath-cleaned fluorine-doped tin oxide (FTO, TEC 15, Hartford Glass Co.) by spray pyrolysis using 0.2 M titanium diisopropoxide bis(acetylacetonate) in a 1-butanol solution at 450 °C. The TiO$_2$ layer was annealed at 450 °C for 1 h. The perovskite films were prepared using a recently reported

solution-processing method based on a nonstoichiometric precursor.[34] In brief, MAI-rich ~50 wt % precursor (MAI:PbI$_2$ = 1.2:1, molar ratio) was prepared by dissolving MAI (Dyesol) and PbI$_2$ (Alfa) in a mixed solvent comprising a mixture of *N*-methyl-2-pyrrolidinone (NMP)/γ-butyrolactone (GBL) (7:3, weight ratio) solvent. Wet precursor film was dispersed on top of a substrate by spin-coating at 4500 rpm for 25 s. The substrate was then dipped into a diethyl ether (DEE, Fisher Chemical) bath for about 90 s. After the substrate was removed from the DEE bath, the substrate was dried with N$_2$ flow, followed by thermal annealing covered under a Petri dish on a hot plate at 150 °C for about 5−10 min.

XPS. Experiments were performed in a Physical Electronics photoelectron spectrometer under UHV conditions (2×10^{-10} Torr). Excitation was provided from monochromatic Al Kα X-rays. The 2 mm Al anode was continuously operated at 350 W. Sample orientation was 45° from the X-ray source and photoelectron detector. Pass energy was 29.35 eV. Multipoint binding-energy calibration followed values reported by Seah for Au 4f$_{7/2}$, Ag 3d$_{5/2}$, and Cu 2p$_{3/2}$ core-level centroids.[35] For the studies reported here, we determined that the preparation of the MAPbI$_3$ using a modified one-step process effectively suppressed PbI$_2$ nucleation for up to 1 week in UHV conditions. Through the suppression of MAPbI$_3$ decomposition processes associated with UHV conditions, a thorough study of the impact of X-ray exposure of MAPbI$_3$ films was made possible.

UV−Vis. A Cary 6000i spectrophotometer equipped with an integrating sphere was used to measure transmission spectra of samples identical to those used in the XPS studies. Three sample spots having been exposed to X-ray during XPS measurements under the same conditions were measured.

XRD. X-ray diffraction data was measured on a Rigaku rotating anode system using a Cu target and a monochromator to select Cu Kα radiation. Data was acquired on the same sample over the course of several days with no substantive difference found for a sample stored in the dark in air or in N$_2$.

■ ASSOCIATED CONTENT

Ⓢ Supporting Information

The Supporting Information is available free of charge on the ACS Publications website at DOI: 10.1021/acsenergy-lett.6b00196.

 Additional information including XPS analysis, XRD data, and UV−vis spectra (PDF)

■ AUTHOR INFORMATION

Corresponding Authors
*E-mail: kenneth.steirer@nrel.gov.
*E-mail: joseph.berry@nrel.gov.

Notes
The authors declare no competing financial interest.

■ ACKNOWLEDGMENTS

■ REFERENCES

(1) NREL. Best Research-Cell Photovoltaic Efficiency Chart. https://upload.wikimedia.org/wikipedia/commons/archive/3/35/20160317201049%21Best_Research-Cell_Efficiencies.png (accessed April 13, 2016).

(2) Berry, J.; Buonassisi, T.; Egger, D.; Hodes, G.; Kronik, L.; Loo, Y. L.; Lubomirsky, I.; Marder, S. R.; Mastai, Y.; Miller, J. S.; et al. Hybrid Organic−Inorganic Perovskites (HOIPs): Opportunities and Challenges. *Adv. Mater.* **2015**, *27*, 5102−5112.

(3) Mei, A.; Li, X.; Liu, L.; Ku, Z.; Liu, T.; Rong, Y.; Xu, M.; Hu, M.; Chen, J.; Yang, Y.; et al. A hole-conductor−free, fully printable mesoscopic perovskite solar cell with high stability. *Science* **2014**, *345*, 295−298.

(4) Sanehira, E. M.; Tremolet de Villers, B. J.; Schulz, P.; Reese, M. O.; Ferrere, S.; Zhu, K.; Lin, L. Y.; Berry, J. J.; Luther, J. M. Influence of Electrode Interfaces on the Stability of Perovskite Solar Cells: Reduced Degradation Using MoO$_x$/Al for Hole Collection. *ACS Energy Letters* **2016**, 38.

(5) Schulz, P.; Dowgiallo, A.-M.; Yang, M.; Zhu, K.; Blackburn, J. L.; Berry, J. J. Charge Transfer Dynamics between Carbon Nanotubes and Hybrid Organic Metal Halide Perovskite Films. *J. Phys. Chem. Lett.* **2016**, *7*, 418−425.

(6) Zhang, S. B.; Wei, S.-H.; Zunger, A. Stabilization of Ternary Compounds via Ordered Arrays of Defect Pairs. *Phys. Rev. Lett.* **1997**, *78*, 4059−4062.

(7) Yang, J.-H.; Yin, W.-J.; Park, J.-S; Wei, S.-H. Self-regulation of charged defect compensation and formation energy pinning in semiconductors. *Sci. Rep.* **2015**, *5*, 16977.

(8) Brivio, F.; Butler, K. T.; Walsh, A.; van Schilfgaarde, M. Relativistic quasiparticle self-consistent electronic structure of hybrid halide perovskite photovoltaic absorbers. *Phys. Rev. B: Condens. Matter Mater. Phys.* **2014**, *89*, 155204.

(9) Yang, Y.; Ostrowski, D. P.; France, R. M.; Zhu, K.; van de Lagemaat, J.; Luther, J. M.; Beard, M. C. Observation of a hot-phonon bottleneck in lead-iodide perovskites. *Nat. Photonics* **2015**, *10*, 53−59.

(10) Brandt, R. E.; Stevanovic, V.; Ginley, D. S.; Buonassisi, T. Identifying defect-tolerant semiconductors with high minority-carrier lifetimes: beyond hybrid lead halide perovskites. *MRS Commun.* **2015**, *5*, 265−275.

(11) Zakutayev, A.; Caskey, C. M.; Fioretti, A. N.; Ginley, D. S.; Vidal, J.; Stevanovic, V.; Tea, E.; Lany, S. Defect Tolerant Semiconductors for Solar Energy Conversion. *J. Phys. Chem. Lett.* **2014**, *5*, 1117−1125.

(12) Walsh, A.; Scanlon, D. O.; Chen, S.; Gong, X. G.; Wei, S.-H. Self-Regulation Mechanism for Charged Point Defects in Hybrid Halide Perovskites. *Angew. Chem., Int. Ed.* **2015**, *54*, 1791−1794.

(13) Yin, W.-J.; Shi, T.; Yan, Y. Unusual defect physics in CH$_3$NH$_3$PbI$_3$ perovskite solar cell absorber. *Appl. Phys. Lett.* **2014**, *104*, 063903.

(14) Eames, C.; Frost, J. M.; Barnes, P. R. F.; O'Regan, B. C.; Walsh, A.; Islam, M. S.; et al. Ionic transport in hybrid lead iodide perovskite solar cells. *Nat. Commun.* **2015**, *6*, 7497.

(15) Chen, S.; Yang, J.-H.; Gong, X. G.; Walsh, A.; Wei, S.-H. Intrinsic Point Defects and Complexes in the Quaternary Kesterite Semiconductor Cu$_2$AnSnS$_4$. *Phys. Rev. B: Condens. Matter Mater. Phys.* **2010**, *81*, 245204.

(16) Xu, R.; Xu, H.-T.; Tang, M.-Y.; Wang, L.-J. Hybrid Density Functional Studies of Cadmium Vacancy in CdTe. *Chin. Phys. B* **2014**, *23*, 077103.

(17) Zhang, Y. Y.; Chen, S.; Xu, P.; Xiang, H.; Gong, X.-G.; Walsh, A.; Wei, S.-H. Intrinsic Instability of the Hybrid Halide Perovskite Semiconductor CH$_3$NH$_3$PbI$_3$. Unpublished work, 2015; http://arxiv.org/pdf/1506.01301v1, pp 1−11.

(18) Matsumoto, F.; Vorpahl, S. M.; Banks, J. Q.; Sengupta, E.; Ginger, D. S. Photodecomposition and Morphology Evolution of

Organometal Halide Perovskite Solar Cells. *J. Phys. Chem. C* **2015**, *119*, 20810−20816.

(19) Ndione, P. F.; Yin, W. J.; Zhu, K.; Wei, S. -H; Berry, J. J. Monitoring the stability of organometallic perovskite thin films. *J. Mater. Chem. A* **2015**, *3*, 21940−21945.

(20) Xiao, C.; Li, Z.; Guthrey, H.; Moseley, J.; Yang, Y.; Wozny, S.; Moutinho, H.; To, B.; Berry, J. J.; Gorman, B.; et al. Mechanisms of Electron-Beam-Induced Damage in Perovskite Thin Films Revealed by Cathodoluminescence Spectroscopy. *J. Phys. Chem. C* **2015**, *119*, 26904−26911.

(21) Alberti, A.; Deretzis, I.; Pellegrino, G.; Bongiorno, C.; Smecca, E.; Mannino, G.; Giannazzo, C.; et al. Similar Structural Dynamics for the Degradation of $CH_3NH_3PbI_3$ in Air and in Vacuum. *ChemPhysChem* **2015**, *16*, 3064−3071.

(22) Philippe, B.; Park, B.-W.; Lindblad, R.; Oscarsson, J.; Ahmadi, S.; Johansson, E. M. J.; Rensmo, H. Chemical and Electronic Structure Characterization of Lead Halide Perovskites and Stability Behavior under Different Exposures - A Photoelectron Spectroscopy Investigation. *Chem. Mater.* **2015**, *27*, 1720−1731.

(23) Schulz, P.; Whittaker-Brooks, L. L.; MacLeod, B. A.; Olson, D. C.; Loo, Y.-L.; Kahn, A. Electronic Level Alignment in Inverted Organometal Perovskite Solar Cells. *Adv. Mater. Interfaces* **2015**, *2*, 1400532.

(24) Emara, J.; Schnier, T.; Pourdavoud, N.; Riedl, T.; Meerholz, K.; Olthof, S. Impact of Film Stoichiometry on the Ionization Energy and Electronic Structure of $CH_3NH_3PbI_3$ Perovskites. *Adv. Mater.* **2016**, *28*, 553−559.

(25) Shkrob, I. A.; Marin, T. W. Charge Trapping in Photovoltaically Active Perovskites and Related Halogenoplumbate Compounds. *J. Phys. Chem. Lett.* **2014**, *5*, 1066−1071.

(26) Calloni, A.; Abate, A.; Bussetti, G.; Berti, G.; Yivlialin, R.; Ciccacci, F.; Duo, L. Stability of Organic Cations in Solution-Processed $CH_3NH_3PbI_3$ Perovskites: Formation of Modified Surface Layers. *J. Phys. Chem. C* **2015**, *119* (37), 21329−21335.

(27) Liu, L.; McLeod, J. A.; Wang, R.; Shen, P.; Duhm, S. Tracking the formation of methylammonium lead triiodide perovskite. *Appl. Phys. Lett.* **2015**, *107*, 061904.

(28) Avrami, M. Granulation, Phase Change, and Microstructure Kinetics of Phase Change. III. *J. Chem. Phys.* **1941**, *9*, 177.

(29) Du, Z. H.; Zhang, T. S.; Zhu, M. M.; Ma, J. Perovskite crystallization kinetics and dielectric properties of the PMN-PT films prepared by polymer-modified sol-gel processing. *J. Mater. Res.* **2009**, *24*, 1576−1584.

(30) Schulz, P.; Edri, E.; Kirmayer, S.; Hodes, G.; Cahen, D.; Kahn, A. Interface energetics in organo-metal halide perovskite-based photovoltaic cells. *Energy Environ. Sci.* **2014**, *7*, 1377−1381.

(31) Miller, E. M.; Zhao, Y.; Mercado, C. C.; Saha, S. K.; Luther, J. M.; Zhu, K.; Stevanovic, V.; Perkins, C. L.; van de Lagemaat, J. Substrate-controlled band positions in $CH_3NH_3PbI_3$ perovskite films. *Phys. Chem. Chem. Phys.* **2014**, *16*, 22122−22130.

(32) Yuan, Y.; Chae, J.; Shao, Y.; Wang, Q.; Xiao, Z.; Centrone, A.; Huang, J. Photovoltaic Switching Mechanism in Lateral Structure Hybrid Perovskite Solar Cells. *Adv. Energy Mater.* **2015**, *5*, 1500615.

(33) Ruiz-Morales, J. C.; Canales-Vazquez, J.; Savaniu, C.; Marrero-Lopez, D.; Zhou, W.; Irvine, J. T. S. Disruption of extended defects in solid oxide fuel cell anodes for methane oxidation. *Nature* **2006**, *439*, 568−571.

(34) Yang, M.; Zhou, Y.; Zeng, Y.; Jiang, C.-S.; Padture, N. P.; Zhu, K. Square-Centimeter Solution-Processed Planar $CH_3NH_3PbI_3$ Perovskite Solar Cells with Efficiency Exceeding 15%. *Adv. Mater.* **2015**, *27*, 6363−6370.

(35) Seah, M. P. Post-1989 Calibration Energies for X-ray Photoelectron Spectrometers and the 1990 Josephson Constant. *Surf. Interface Anal.* **1989**, *14*, 488.